

**Molecular Gas and Star Formation in the
Host Galaxy of the QSO I Zw 1**

E. Schinnerer, A. Eckart, L.J. Tacconi

Max Planck Institut für extraterrestrische Physik, 85740 Garching, Germany

arXiv:astro-ph/9801061v1 8 Jan 1998

to appear in *Astrophysical Journal* (accepted)

Received _____; accepted _____

ABSTRACT

We have investigated the ISM of the I Zw 1 QSO host galaxy with Plateau de Bure mm-interferometry and high angular resolution near-infrared imaging spectroscopy. We have detected a circumnuclear gas ring of diameter $\sim 1.5''$ (~ 1.8 kpc) in its millimetric CO line emission and have mapped the disk and the spiral arms of the host galaxy in the $^{12}\text{CO}(1-0)$ line at 115 GHz as well as in the H ($1.65 \mu\text{m}$) and K ($2.2 \mu\text{m}$) band. Combining our new mm- and NIR-data with available estimates of the radio- and far-infrared contributions to the nuclear emission, we find strong evidence for a nuclear starburst ring. A comparison to other sources with nuclear activity indicates that these rings may be a common phenomenon and contribute a large fraction of the central luminosity.

Both the CO rotation curve as well as the NIR and optical images are consistent with an inclination of $(38\pm 5)^\circ$. Using this we obtain a total dynamical mass of $(3.9\pm 1.6)\times 10^{10} M_\odot$ and a cold molecular gas mass of $(7.5\pm 1.5)\times 10^9 M_\odot$ for the inner 3.9 kpc. With an estimate of the nuclear stellar contribution to the mass and light from NIR spectroscopy and assuming that the contribution of the HI gas to the overall mass of the inner 3.9 kpc is small we derive an $\frac{N_{\text{H}_2}}{I_{\text{CO}}}$ -conversion factor close to $2\times 10^{20} \text{cm}^{-2} \text{K}^{-1} \text{km}^{-1} \text{s}$ found for molecular gas in our Galaxy and many nearby external galaxies.

A comparison to broad band spectra of spiral galaxies, ellipticals and the nucleus and disk in NGC 7469 suggests bluer disk colors for I Zw 1, and that star formation in the host galaxy and the western companion of I Zw 1 is enhanced. This is also supported by a starburst analysis using all available data on the northwestern spiral arm. The presence of molecular material within the disk and on the arm indicates that at least in this region 12 kpc from the nucleus star formation, and not scattered light from the QSO nucleus, is responsible for the blue disk colors.

Subject headings: galaxies: ISM - galaxies: hosts - galaxies: stellar content - quasars: individual (I Zw 1)

1. INTRODUCTION

Recent investigations of bright active galactic nuclei have shown that the starburst phenomenon contributes a major fraction of the total luminosity of these sources (Genzel et al. 1997). In addition several models suggest evolutionary links between different classes of extragalactic sources (e.g. Osterbrock 1993, Norman and Scoville 1988, Sanders et al. 1988, Rieke, Lebofsky & Walker 1988). A key test of these evolutionary sequences is to investigate the structure and concentration of the molecular material as well as the distribution and composition of the stellar population in the nuclei and circumnuclear regions of a sample of galaxies representing the different classes. Several luminous and ultra-luminous extragalactic nuclei have been observed with high angular resolution, and have shown the presence of circumnuclear starburst rings. These rings, therefore, deserve special attention since they are important tracers of the dynamics and star formation in active and luminous galactic nuclei. Due to the combined requirement of high spatial resolution and sensitivity these investigations become increasingly difficult when going to larger distances. In the course of such a systematic effort we present new results we have obtained with imaging and spectroscopy on the nearby QSO I Zw 1.

I Zw 1, at a redshift of $z=0.0611$ (Condon et al. 1985), is thought to be the closest QSO because of its high optical nuclear luminosity ($M_V=-23.8^{mag}$ Véron-Cetty & Véron 1991). For this redshift its distance is 244 Mpc assuming $H_o=75 \text{ kms}^{-1}\text{Mpc}^{-1}$. I Zw 1 shows spectral properties of high-redshift QSOs (e.g. CIV ($\lambda 1549\text{\AA}$) which are blueshifted by 1350 km/s (Buson & Ulrich 1990)). It also has a high X-ray luminosity (Krupe et al. 1990, Boller, Brandt & Fink 1996). I Zw 1 is the prototype object of the Narrow-Line Seyfert 1 (NLS1) class. The FWHM of the $H\beta$ line is $\approx 1240 \text{ km/s}$, the OIII/ $H\beta$ ratio is smaller than 3 and strong optical FeII multiplets are detected (Halpern & Oke 1987). The host galaxy disk has been detected in the V, R and H band (Bothun et al. 1984, Hutchings & Crampton 1990, McLeod & Rieke 1995), and its molecular gas has been observed in the $^{12}\text{CO}(1-0)$ (Barvainis et al. 1989), $^{12}\text{CO}(2-1)$ and $^{13}\text{CO}(1-0)$ lines (Eckart et al. 1994). The two objects seen near the edges of the disk are a foreground star to the north, and a companion galaxy to the west (Hutchings & Crampton 1990). The QSO nucleus is located in a gas rich host galaxy disk, which makes I Zw 1 an ideal candidate for studying the properties of QSO hosts.

We present the observations and data reduction in section 2 and discuss the distribution, mass and dynamics of the molecular gas in section 3. The near-infrared imaging and spectroscopy results are given in section 4, and the possibility of a massive nuclear starburst (section 5) is then followed by a comparison with other starburst rings (section 6). In section 7 we compare the optical/near-infrared broad band spectra of the northwestern spiral arm in the I Zw 1 host galaxy and the western companion to those of spiral galaxies, ellipticals and the disk and nucleus of NGC 7469. We give a summary and conclusions in section 8.

2. OBSERVATIONS AND DATA REDUCTION

2.1. Millimeter-Spectroscopy

We have mapped the ^{12}CO J=1-0 line emission in I Zw 1 in January/February 1995 with the IRAM millimeter interferometer on the Plateau de Bure, France (Guilloteau et al. 1992). The four 15 m antennas were positioned in four different configurations, providing 24 baselines, ranging from 24 m to 288 m length. The antennas were equipped with SIS receivers with single-sideband (SSB) system temperatures above the atmosphere of 170 K. The observed frequency was 108.633 GHz due to the redshift $z=0.0611$ of I Zw 1 (Condon et al. 1985). $3\text{C } 454.3$ was observed for bandpass calibration, while phases and amplitudes were calibrated on 0106+013.

The CO maps were made using the IRAM reduction package CLIC, and were CLEANed with the IRAM reduction package GRAPHIC. The resolution of the synthesized beam was $1.9''$ (uniform weighting), but we made $5''$ resolution CLEAN maps (natural weighting) with spectral resolutions of 10 km/s and 40 km/s to study the extended disk structure and velocity field. For the studies of the core component we used the $1.9''$ resolution CLEANed maps with a spectral resolution of 20 km/s. To investigate the dynamics of the nucleus we calculated velocity maps as well as p-v diagrams along the major and minor kinematic axis of I Zw 1.

2.2. Near-Infrared Spectroscopy and Imaging

I Zw 1 was observed in the K band ($2.20\ \mu\text{m}$) in January 1995 with the MPE imaging spectrometer 3D (Weitzel et al. 1996, Thatte et al. 1995) at the 3.6m telescope in Calar Alto, Spain. The observations in the H band ($1.65\ \mu\text{m}$) were carried out in December 1995 at the William Herschel Telescope in La Palma, The Canary Islands.

For both sets of observations the image scale was $0.5''/\text{pixel}$. The total integration time on source was 4200 s for the K band and 1530 s for the H band.

3D obtains simultaneous spectra ($R \equiv \lambda/\Delta\lambda \approx 1000$ for H band and 750 for K band) of an $8'' \times 8''$ field. This is done using an image slicer which rearranges the two-dimensional focal plane onto a long slit of a grism. The dispersed spectra are then detected on a NICMOS 3 array. A detailed description of the instrument and the data reduction are given in Weitzel et al. (1996). The data reduction procedure converts each two dimensional image into a three dimensional data cube with two spatial axes and one spectral axis. The data cubes are coadded after rebinning onto a $0.25''$ grid and centered on the continuum peak. All images are dark-current and sky-background subtracted, corrected for dead and hot pixels, and spatially and spectrally flatfielded. To correct the effects of the Earth's atmosphere to the K band spectrum, a standard star was observed. This standard spectrum was first divided by a template spectrum of the same spectral type (Kleinmann & Hall 1986) in order to remove stellar features. For the region of the central ($1.522 - 1.714\ \mu\text{m}$) H band we used a model atmosphere, because currently no H band template spectra are available

at our spectral resolution. The model atmosphere for the atmospheric correction in the H band was calculated via ATRAN (Lord 1992). At the H band edges, however, the model atmosphere spectrum was substituted with the atmospheric transmission derived via the standard star, since this is probably more reliable, and the standard star does not show strong features in these wavelength ranges. The effect due to different zenith distance of source and standard star in H and K band was minimized using the ATRAN atmospheric model (Lord 1992), mainly to correct for the different atmospheric absorption. The source data were divided by the atmospheric transmission spectrum. We flux calibrated the data adopting the integrated flux density values given by Edelson & Malkan (1986) for 5" circular apertures centered on the nucleus.

With a larger field of view the H and K band continuum emission of the QSO host galaxy was observed in July 1995 with the ESO IRAC2 camera at the ESO/MPG 2.2m telescope on La Silla, Chile. The image scale was 0.27" per pixel resulting in a 69" × 69" field of view. We applied a correction for the sky background, dead pixels and a flat field to the data. The different frames were coadded using the central peak of the brightness distribution as a reference. Again we adopted the calibration used by Edelson & Malkan (1986) as described above. As determined from images of the compact nucleus, the seeing was about 1.3". For a better comparison to the interferometer maps and to improve the signal-to-noise we convolved the images to a resolution of $\sim 2.4''$.

3. THE PROPERTIES OF THE MOLECULAR GAS

Knowledge of the properties of the molecular gas is essential to the understanding of star formation in and the fueling of AGNs, since molecular clouds are the major reservoir for these phenomena. Interferometry at mm-wavelengths allows high angular resolution dynamical studies of the molecular gas in the vicinity of the active nucleus. For the first time we have detected the molecular line emission in the spiral arms of a QSO host galaxy. In addition we are able to decompose the line emission into a core and disk component. Analyzing the velocity field we have found a circumnuclear ring of molecular gas with similar size to starburst rings found in nearby galaxies. At our spatial resolution of 1.9" (2.2 kpc) we see no obvious sign of gas streaming directly into the very nucleus.

3.1. The Distribution of the Molecular Gas in I Zw 1

Since the molecular gas is the reservoir for the star formation, it is important to investigate its distribution throughout the entire host galaxy. This can shed light on any differences which exist between the star forming processes in the host galaxy disk and those of the nuclear region. Therefore we made integrated CO emission maps (Fig.1) at spatial resolutions of 1.9" and 5.0", using only emission exceeding the 3σ level in each channel. The nuclear peak in the CO emission shows an offset of 1" compared to the VLA coordinates,

probably due to differences of the interferometer phase centers of the PdBI and the VLA. In the 5" spatial resolution map we detect two spiral arms to the west and east of the nucleus (Fig.1 and 2 (Plate 1)). In the high resolution map these arms are apparent at the lowest contour level. The extended line emission from the host galaxy is resolved out at high resolution. The northwestern spiral arm has also been seen in optical and infrared broad-band images (see section 7). We also find a smooth disk with an extent of 20" EW and 13" NS. As shown in Fig.1 most of the flux originates in the central 9". In the 5" resolution map the nucleus has a FWHM of 6", which results in an intrinsic diameter of about 3.3" after deconvolution with the CLEAN beam at a spatial resolution of 5". In the 1.9" resolution map the FWHM diameter of the core is about 3", resulting in an intrinsic diameter of 2.3". Also the integral in a 5.5" × 5.5" box centered on the nucleus in the 5" resolution map equals 10 Jy km s⁻¹ whereas the integral in a 2" × 2" box in the 1.9" resolution map results in a flux of about 5 Jy km s⁻¹. The two measurements clearly indicate the presence of a more extended component, which is partially resolved in both maps. This shows that the interferometer data may not contain all of the total flux of the source. This is also supported by a comparison to IRAM 30 m data as shown in the following section.

3.1.1. *Decomposing the ¹²CO Line Emission*

We have compared the spectrum taken by Barvainis et al. (1989) with the IRAM 30m telescope with a total spectrum of our IRAM PdBI Interferometer observations to derive the overall extended line flux emitted by the disk of the I Zw 1 host galaxy. Both spectra show a double horned profile, with the 30m spectrum having more flux in the horns. In double horned line profiles the emission in the horns is dominated by an extended disk component. In addition the 30 m beam size is smaller than the optical disk size and of the same order as (or as well smaller than) the structure of the CO line emission measured with the PdBI interferometer. This indicates that our observations as well as the 30 m observations have missed some flux from the disk. The amount of flux missed by the two observations depends on the disk size, shape and assumed model (see below and section 3.1.2). To decompose the flux into a nuclear and a disk component we estimated the contribution of the compact 3.3" FWHM core (we measured with the PdBI) to the total flux (0.078 Jy, value measured between the two horns) of the 30 m telescope (Barvainis et al. 1989). From our low resolution ¹²CO (1-0) map we measure a FWHM of the nuclear component of about 3.3" and a peak flux of 0.040 Jy close to the systemic velocity of I Zw 1. As defined below we used correction factors F_G and F_D that have to be applied to the measured flux for the beam filling under the assumption that beam and source are both circular and the beam has a Gaussian profile (Dickel 1976).

If the intensity distribution of the source is Gaussian, we get

$$F_G = \frac{(\theta_{FWHM})^2}{(\theta_B)^2} = \frac{(\theta_B)^2 + (\theta_S)^2}{(\theta_B)^2} = 1 + \left(\frac{\theta_S}{\theta_B}\right)^2 \quad (1)$$

where θ_S and θ_B are the FWHM of the source and the beam. If the intensity distribution of the source is flat and disk-like (Heeschen 1961), we obtain

$$F_D = \frac{\ln 2 \cdot \left(\frac{\theta_S}{\theta_B}\right)^2}{1 - \exp(-\ln 2 \cdot \left(\frac{\theta_S}{\theta_B}\right)^2)} \quad (2)$$

where θ_S is the diameter of the uniform disk and θ_B is the FWHM of the beam. Using the beam filling correction factors calculated from the known PdBI and 30m beams and assuming a Gaussian nuclear source size of 3.3" we find that the nucleus accounts for 0.056 Jy, i.e. 70% of the total line flux measured by the 30m telescope. We, therefore, decomposed the 30m line flux into a nuclear (0.056 Jy) and a disk (0.022 Jy) component. The decomposition is consistent with the source extents and structures found in the channel maps (Fig.1, 2 and 3), and in optical and NIR-images. Alternatively the PdBI and 30m spectra only match if we assume unrealistically high calibration errors $\geq 20\%$ for both observed values, with the 30 m flux being too high and the PdBI flux being too low.

3.1.2. Size of the Host Galaxy in the ^{12}CO Line Emission

Assuming a disk flux of 0.022 Jy, we derive its size, since we have two measurements at different angular resolutions. For the disk we assume both Gaussian and flat intensity distributions. The value of the background noise in the single channel maps is of the order of 0.006 Jy (3σ level). This value was used together with the disk flux to estimate a lower limit to the spatial extent of the disk via the beam filling factors. For a Gaussian (flat) flux distribution we get a disk diameter of 9" (12") or higher taking into account that parts of the extended emission might also have been missed by the 30 m measurements. This is in good agreement with the upper limit in disk size of about 30" obtained from optical and NIR observations. This is especially true if we consider the extended wings in case of a more realistic Gaussian distribution. The molecular disk size of the host galaxy should have an extent of about 10 kpc (or larger), compared to that of the bright core component with a FWHM of 3.3" or about 3.9 kpc.

3.2. The Dynamics of the Molecular Gas in I Zw 1

Our $^{12}\text{CO}(1-0)$ spectrum shows a double-horn profile characteristic of rotating disks, and is similar to the CO spectra of I Zw 1 presented in Barvainis et al. (1989) and Eckart et al. (1994). The rotation of the extended disk emission is obvious in the channel maps (Fig.3). From the mean velocity field (Fig.4) we measure a kinematic major axis position angle of 135° . The velocity field shows no signs of a very strong interaction with the western

companion. This companion is not detected at our S/N level of 0.006 Jy.

In Fig.5 we present the position-velocity diagrams along the major kinematic axis for the two different spatial resolutions. Each half of the p-v diagram represents the projected rotation curve for I Zw 1.

3.2.1. *Inclination*

The exact inclination of the I Zw 1 host galaxy is not known, although the optical and NIR-images indicate a fairly low inclination of $\sim 40^\circ$ (Bothun et al. 1984). To test this value for the inclination kinematically we assumed a typical disk rotation velocity of (250 ± 25) km/s (Rubin et al. 1985) for the flat part of the rotation curve (at a distance of about $10''$) assuming this is characteristic of motions in the disk. From this we derive an inclination in the range of $(34\pm 4)^\circ$ depending on the chosen rotation velocity. This value is in approximate agreement with the shape of the 50% contour lines in the maps in Fig.1 under the assumption that the CO line emission has an intrinsically azimuthally symmetric distribution. As a compromise we have chosen a value of $(38\pm 5)^\circ$ which would be consistent with a rotation velocity of (230 ± 30) km/s for the disk. This value, as well as the position angle of the major axis of 135° that we get from the CO velocity field are in agreement with the observed ellipticity of the R band image (Hutchings & Crampton 1990) assuming an intrinsically circular disk.

3.2.2. *pv-Diagrams*

The p-v diagrams show evidence for a circumnuclear ring, extended disk emission and the presence of a large molecular cloud complex located close to the nucleus. In the following we will summarize observational properties of these regions:

The circumnuclear ring: The pv-diagram (Fig.5a) made at $1.9''$ angular resolution has two flux peaks at velocities of ± 180 km/s, indicating the presence of a nuclear ring or spiral arms, with a diameter of about $1.6''$. The nuclear velocity dispersion was measured in a pv-diagram along the kinematic minor axis. The values given below are the 50% contour widths corrected for the spectral resolution. The intrinsic velocity dispersion is estimated assuming a Gaussian velocity distribution. The nuclear source exhibits a high velocity dispersion of $\sigma=350$ km/s, assuming that the gas is isothermal and that the velocity dispersion is radius independent for radii less than $2''$. This is also clearly demonstrated and supported by the pv-diagrams along the minor axis (Fig.5). However, the σ derived above may not only be due to pure cloud-cloud velocity dispersion but may also contain contributions from a more complex velocity field like a tilted ring system as in Centarus A (Nicholson et al. 1992, Quillen et al. 1992, 1993, Sparke 1996) or streaming motions.

The GMC complex: The single emission peak at a velocity of 220 km/s and approximately $2''$ E and $2''$ S of the nucleus could be due to a molecular gas complex located in or near the

nuclear ring. This GMC complex also appears in the low spatial resolution map (Fig.5c). It seems to be kinematically unresolved, indicating a small velocity dispersion of about 20 km/s, similar to what is observed for GMC complexes in our Galaxy. The molecular mass contained in this complex (estimated from the CO luminosity read off from the pv-diagrams in Fig.5) is $\sim 5\%$ of the total nuclear molecular gas mass. This is one order of magnitude higher than that measured for GMC complexes in our Galaxy.

The disk emission: The flat part of the rotation curve levels out at velocities of ± 140 km/s. Our S/N ratio enables us to trace the extended disk emission out to radii of 18 kpc. The velocity dispersion of the disk component is ~ 17 km/s.

Modelling the p-v diagrams: We have calculated model pv-diagrams to improve our understanding of the structure and dynamics of the nucleus and the disk of I Zw 1 (see Fig. 5). The model projects a given galaxy flux geometry onto a sky grid taking inclination and tilt into account. To this flux geometry a rotation curve is applied. The beam size and velocity resolution of the observation are then used to calculate the model pv-diagram. To model the molecular gas emission in I Zw 1 we assumed a two component Gaussian flux distribution. One Gaussian had a FWHM of $10''$ centered at a radius of $4''$ and the other a FWHM of $1.65''$ centered at a radius of $0.8''$. The ratio between the two Gaussian flux peaks was 50 with the inner one being the brighter one. This model flux distribution is plotted in Fig.6.

The azimuthally symmetric modelled p-v diagrams match the measured ones very well, except that they do not reproduce emission from the single GMC complex. Also they account only approximately for the emission of the disk component. The remaining differences between the data and the model are due to the presence of spiral arms in the observed maps (see Fig.1). The modelled p-v diagrams do demonstrate the need of a circumnuclear ring-like distribution of the molecular gas, as well as the need for a high velocity dispersion in the nuclear source. This high velocity dispersion could be due to gas streaming along a bar, because the nuclear emission in the velocity field (Fig.4) is slightly S-shaped as one would expect for streaming (Sanders & Tubbs 1980, Tacconi et al. 1994).

3.3. The Mass of the Molecular Gas in I Zw 1

Since the molecular gas mass is a substantial part of the dynamical mass, it is essential to know its distribution and mass. With velocity widths of 380 km/s for the nucleus and 310 km/s (distance horn-to-horn) for the disk and a $\frac{N_{H_2}}{I_{CO}}$ -conversion factor of $2.0 \times 10^{20} \frac{cm^{-2}}{K kms^{-1}}$ (Strong et al. 1987), we get a molecular gas mass for the nuclear component of $7.5 \times 10^9 M_\odot$, and of $2.7 \times 10^9 M_\odot$ for the Gaussian disk and $0.7 \times 10^9 M_\odot$ for the flat disk (see Table 1 and 2). From the rotation curve we derive a dynamical mass for the central region ($3.3''$ FWHM) of $(3.9 \pm 1.6) \times 10^{10} M_\odot$, assuming a rotation velocity of (290 ± 60) km/s for the nuclear component. The molecular mass is then about $\sim 20\%$ of the dynamical mass in the nucleus. This is at the upper end of what is expected for normal spiral galaxies (typical values are 5 -10%; e.g. McGaugh & de Blok, 1997).

The $\frac{N_{H_2}}{I_{CO}}$ -conversion factor: Given estimates of the dynamical and stellar masses in the nucleus we are able to test the $\frac{N_{H_2}}{I_{CO}}$ -conversion factor. This factor was calculated for molecular clouds in our Galaxy (e.g. Strong et al. 1987, van Dishoeck & Black 1987 and references therein) and seems to be constant within a factor of two for ensembles of molecular clouds in other galaxies (e.g. Xie, Young, Schloerb 1994, Eckart et al. 1990, 1991, Eckart 1996, Wilson & Reid 1991, Tacconi et al. 1997, Solomon et al. 1997, but see also Maloney and Black 1988). The standard conversion factor ($2.0 \times 10^{20} \frac{cm^{-2}}{K km s^{-1}}$; Strong et al. 1987) results in a molecular gas mass for the nuclear component of $M_{H_2} = (7.5 \pm 1.5) \times 10^9 M_\odot$. The total dust mass is only a few times $10^7 M_\odot$ (Eckart et al. 1994) and can be neglected in the following. We used the dynamical mass of $M_{DYN} = (3.9 \pm 1.5) \times 10^{10} M_\odot$ derived from the rotation curve and the stellar mass of the starburst of $M_{ST} = (1.9 \pm 0.7) \times 10^{10} M_\odot$ (see section 4). Correcting for helium (36 % of the molecular gas mass) we can now test the conversion factor via

$$\frac{M_{DYN} - M_{ST} - 0.36 M_{H_2}}{M_{H_2}} = \frac{M_{DYN} - M_{ST}}{M_{H_2}} - 0.36 = 2.3 \pm 1.4 \quad (3)$$

We find the $\frac{N_{H_2}}{I_{CO}}$ -conversion factor to agree within the errors with the canonical value of $2 \times 10^{20} \frac{cm^{-2}}{K km s^{-1}}$ (Strong et al. 1987). Remaining differences can easily be explained by uncertainties in our assumptions of the temperatures of the gas, the geometry assumed in calculating the dynamical mass, a higher fraction of warm molecular gas and also by an old bulge population of late type stars which contributes approximately 2% of the reddened stellar contribution to the K band flux equals 1% of the overall nuclear K band flux. Such an old stellar population would have a mass of about $10^{10} M_\odot$ (Thronson & Greenhouse 1988) and a luminosity of about $4 \times 10^8 L_\odot$. The contribution of this old population cannot be substantially larger than 2% of the reddened stellar K band flux (or even account for all of it) without exceeding the total dynamical mass (see section 5.2).

Our result on I Zw 1 and the findings for other lower redshift galaxies indicate that to within a factor of a few the average $\frac{N_{H_2}}{I_{CO}}$ -conversion factor is valid in these extragalactic objects as well. However, deviations may occur in low metallicity systems or in the presence of substantial amounts of optically thin molecular gas. In the metal-poor dwarf irregular galaxy IC 10 Wilson and Reid (1991) find a conversion factor about twice as large as the Galactic value in disagreement with predictions that the conversion factor should be a strong function of metallicity. In the SMC the conversion factor from CO line intensity to hydrogen column density is found to be larger than the Galactic value and to scale with the linear size of the structures as $\chi_{SMC} \approx 9 \times 10^{20} (R/10 \text{ pc})^{0.7} \text{cm}^{-2} (\text{K km s}^{-1})^{-1}$ (Rubio, Lequeux, Boulanger 1993). A recent analysis of multiple CO transitions from the Cloverleaf quasar by Barvainis et al. (1997) indicates that the conversion factor is probably an order of magnitude smaller than the standard value due to the high emissivity of warm CO which is only moderately optically thick.

The late type spiral shape of the I Zw 1 host galaxy indicates normal metallicity (see also optical line ratios in Phillips 1978) and the ^{12}CO and ^{13}CO line ratios and the decomposition of the molecular line emission into a nuclear and disk component (as discussed in Eckart et

al. 1994) indicates that most of the emission is due to warm optically thick (for the nuclear component) and cold or subthermally excited molecular gas (for the disk component). This indicates that models with an almost arbitrarily low conversion factor due to a high emissivity of warm (optically thin or at least only moderately optically thick) molecular gas probably do not apply in the case of I Zw 1.

4. NEAR-INFRARED EMISSION FROM THE NUCLEUS AND THE HOST GALAXY

4.1. Continuum Images

The host galaxy disk is clearly detected in the optical, NIR and in its molecular line emission (see Fig.1, 2 and 7). There are two spiral arms originating east and west from the nucleus. The western spiral arm is detected in the V, R and H band (Bothun et al. 1984, Smith et al. 1986, McLeod & Rieke 1995) and in the ^{12}CO (1-0) line emission (this paper). The knotty structures in this spiral arm have been interpreted as HII regions (Smith et al. 1986), so the emission from this arm is expected to come mainly from newly formed stars. The eastern spiral arm is obvious in the V and I band HST images of I Zw 1 (HST archive, Proposal 2882, P.I. Westphal, and K.D. Borne, private communication). From the CO map, we see that the material for star formation in the galaxy disk is more concentrated in spiral arms. The western spiral arm is located at larger separations from the nucleus than the eastern arm. Both spiral arms are also evident in our IRAC2 H band map (Fig.7), but less pronounced in the K band data. Both images however clearly show the extended central disk as well as the western companion and the foreground star.

4.2. The Nuclear Near-Infrared Spectrum

We present an H and K band (1.58 - 2.40 μm) NIR-spectrum of the nuclear region (3.0" aperture) with a spectral resolution of about $R=1000$ for the H band and $R=750$ for the K band (see Fig.8). The nuclear NIR spectrum of I Zw 1 is dominated by emission from the AGN with only a small contribution from a stellar population. The spectrum shows a flat continuum indicating high extinction and dust emission as one would expect for a QSO. The spectrum is dominated by strong hydrogen recombination lines and also clearly shows the coronal [SiVI] line. We also detected the CO(6-3) overtone bandhead at 1.62 μm which is due to absorption in stellar atmospheres. All these lines originate within the central 2" or are even spatially unresolved at our resolution of about 1".

4.2.1. Emission Lines in the Near-Infrared

The hydrogen recombination lines are produced in the BLR and NLR of the AGN as well as in the HII regions around hot stars. To separate these two possibilities one can look at the spatial distribution of the emission (e.g. NGC 7469, Genzel et al. 1995). The most prominent line in the K band nuclear spectrum of I Zw 1 is the Pa α line at a rest wavelength of $\lambda_o=1.875\mu\text{m}$. Its maximum flux density is 2/3 of the continuum flux density. Br γ and Br δ are two other H-recombination lines detected in the nucleus (see Fig.8). The FWHM of Pa α is 1000 km/s comparable to the FWHM of Br γ at our S/N ratio. The FWZP is about 6000 km/s although the line shape could be affected by an incomplete atmospheric correction, as there is a strong atmospheric absorption feature nearby. This leads to an uncertainty of about 15% in the FWZP. The line ratio of Pa α to Br γ estimated from both the peak fluxes and integral line strengths is 11:1, close to the 12:1 that one would expect for standard HII-regions with case B recombination ($N_e=10^4\text{cm}^{-3}$ and $T=10^4\text{K}$; Osterbrock 1989). The hydrogen recombination line ratios estimated from the R band spectra of Hutchings & Crampton (1990) also do not differ significantly from the theoretical values. Based on these ratios we conclude that there is little or no extinction towards the very nucleus of the QSO.

Other emission lines which are detected are the two coronal emission lines [SiVI] ($\lambda 1.962\mu\text{m}$) and [AlIX] ($\lambda 2.040\mu\text{m}$) (see Table 3), which arise in hot gas ($T_e \sim 10^5\text{-}10^6\text{K}$) ionized by the AGN. They are blueshifted by 1350 km/s relative to the hydrogen recombination lines. Such a blueshift has also been observed in the [CIV] emission line at $\lambda 1549\text{\AA}$ (Buson & Ulrich 1990). This blueshift indicates that these lines could come from an AGN driven outflow. Our observed line flux of [SiVI] is within the limit derived by Eckart et al. (1994). The flux of Kawara et al. (1990) is higher than ours, possibly due to contamination from the nearby H₂ S(3) line being included in their 0.01 μm wide filter. Laor et al. 1997 find in the UV spectrum of I Zw 1 that the blueshift for ion lines increases with their ionization level. They interpret this as an outflowing component in the BLR, where the ionization level increases with velocity. In addition they detected a weak UV absorption system which indicates an outflow with a line of sight velocity of ~ 1870 km/s. Interestingly, Leighly et al. 1997 interpret oxygen absorption features near 1 keV detected in ASCA X-ray spectra as a highly relativistic outflow from the innermost regions in other NLS1 (IRAS 13224-3809, 1H 0707-495, PG 1404+226). It might be interesting to investigate further, whether the outflow in the IR, UV and the X-ray are physically related.

HeI/Br γ -ratio

The HeI(2.058 μm)/Br γ -ratio is sensitive to the effective temperature of the ionizing source and to the electron density (Doyon et al. 1992, Shields 1993), since both lines are supposed to arise around the ionizing source. Since we do not detect the recombination line of HeI (2.058 μm) in our K band nuclear spectrum, we get an upper limit of ~ 0.30 for the ratio using the 3σ error as an upper limit for the HeI line flux. In this case the effective temperature must be either below 38 000 K or above 50 000 K with an electron density of $\sim 10^3\text{ cm}^{-3}$ (Doyon et al. 1992, Shields 1993, Lançon & Rocca-Volmerange 1996). Since the

QSO nucleus shows at short optical wavelengths a strong contribution of blue non-stellar power law emission (Barvainis 1990) the effective temperature should be large and probably be of the order (or exceed) 50 000 K.

4.2.2. Absorption Lines in the Near-Infrared

The most prominent stellar absorption features are the CO bandheads in the H and K band. These lines arise in the atmospheres of late type giants and supergiants which produce most of the stellar NIR emission. Due to the redshift of I Zw 1 we were not able to detect the strong $^{12}\text{CO}(2-0)$ bandhead at $2.29 \mu\text{m}$, as this line was already shifted out of our detector range. In the H band the $^{12}\text{CO}(6-3)$ overtone bandhead is accessible, however. This clearly detected feature indicates a prominent stellar contribution to the continuum light of the nucleus. We used the depth of this line to estimate the fraction of stellar flux in the H band due to late type giants and supergiants. The observed line depth is about $(3.5 \pm 0.5)\%$ of the continuum. This can be compared to $\sim 20\%$ we typically expect for a population of GKM giants/supergiants which dominate the H band light for stellar populations older than 10^7 yrs. Therefore, we estimate that at least $18 \pm 3\%$ of the total flux in the H band is due to GKM giants/supergiants. Although these stars dominate the stellar emission in the H band, about one third of the total stellar flux is contributed by stars of other spectral classes. Therefore we derive that $27 \pm 6\%$ of the H band continuum in a circular $3''$ aperture is of stellar origin.

In the K band the stellar absorption lines of the CaI-triplet (at $2.26 \mu\text{m}$) are normally present in a stellar population of GKM giants/supergiants but not as prominent as the CO bandheads. These absorption lines are only detected close to their 3σ -level in I Zw 1. If we compare the line depth of $2.4 \pm 0.7\%$ to spectra of late type standard stars with a similar resolution (Ali et al. 1995) which have line depths of about 10% , we derive an upper limit of about 24% for the contribution to the stellar emission from this kind of late type stars.

These estimates of the stellar contribution to the NIR light are consistent with other values in the literature. Barvainis (1990) finds about 20% of stellar continuum flux in the K band and about 30% in the H band in his spectral decomposition. Via a NIR color decomposition Eckart et al. (1994) find a K band contribution of 20% with an extinction of $A_V \approx 10^{mag}$. Comparing our stellar H and K fluxes (magnitudes) to the approximate NIR H-K colors of 0.20 (Frogel et al. 1978) of an unextincted stellar population we can confirm an extinction of about 10^{mag} . The Sc colors can be taken as a reference to obtain first order information on the reddening. This is reasonable since the spread in the mean colors for different galaxy types (e.g. Hunt et al. 1997) is small compared to our calibration errors. The distribution of typical giant and dwarf colors - taken as extreme cases of major flux density distributors in the infrared - indicate that the colors of most stellar systems are very similar. As demonstrated via a spectral synthesis analysis in Schinnerer et al. (1997) this argument can also be extended to starburst populations.

The QSO nucleus of I Zw 1 is located within this extincted central stellar component and

the very low extinction in the line of sight towards the nucleus is most likely due to the central outflow (see section 4.2.1).

5. THE CIRCUMNUCLEAR STARBURST RING

The presence of a molecular ring in the circumnuclear region of I Zw 1, the large stellar contribution to the total nuclear light as well as the analysis given by Eckart et al. (1994) indicate that there is a massive starburst in the circumnuclear region of I Zw 1. Although the central AGN could have a substantial effect on the ISM in the I Zw 1 host galaxy we concentrate in the present paper on an interpretation in which we demonstrate that most of the ISM and stellar disk properties can be accounted for by star formation activity. We use the new data presented in this paper together with a starburst model in order to investigate the properties of the starburst. The K band luminosity L_K , the bolometric luminosity L_{bol} , the Lyman continuum luminosity L_{Lyc} and the supernova rate ν_{SN} are used as observational parameters that are fitted by the model to explain the starburst age, history and upper mass cut-off. In this section we describe the starburst model, the derived the input parameters, and the results of the modeling.

5.1. The Starburst Model

To derive the properties of a starburst from the observed continuum and line intensities we have used the starburst code STARS (Kovo & Sternberg 1997). This model has been successfully applied to NGC 1808 (Krabbe et al. 1994, Tacconi-Garman et al. 1996), NGC 7469 (Genzel et al. 1995), NGC 6764 (Eckart et al. 1996) and NGC 7552 (Schinnerer et al. 1997). A description of the model can be found in the appendices of Krabbe et al. (1994) and Schinnerer et al. (1997) and also in Kovo & Sternberg (1997). The model is similar to other stellar population synthesis models (Larson & Tinsley 1978, Rieke et al. 1980, Gehrz, Sramek & Weedman 1983, MasHesse & Kunth 1991, Rieke et al. 1993, Doyon, Joseph & Wright 1994) and includes the most recent stellar evolution tracks (Schaerer et al. 1993, Meynet et al. 1994).

We assume power-law IMFs which vary as $M^{-\alpha}$ between a lower and upper mass cut-off, m_l and m_u , with an index $\alpha=2.35$ (Leitherer 1996, Salpeter et al. 1955). STARS has as output observable parameters such as the bolometric luminosity L_{bol} , the K band luminosity L_K , the Lyman continuum luminosity L_{Lyc} and the supernova rate ν_{SN} , as well as the diagnostic ratios between these quantities: L_{bol}/L_{Lyc} , L_K/L_{Lyc} and $10^9\nu_{SN}/L_{Lyc}$. All three ratios are measures of the time evolution and the shape of the IMF, with slightly different dependencies on α and m_u . H-R diagrams representing the distribution of these luminosities are calculated. The total number of stars of different stellar type is also calculated. To derive a total stellar mass we integrated over the IMF represented by this H-R diagram.

There is no straightforward way to measure the bolometric luminosity of the central

region of I Zw 1. There are, however, two methods to estimate L_{bol} , and both result in comparable values that are in good agreement with the spectral decomposition by Barvainis (1990). *Firstly* we can use the the CO-FIR relation (Young and Scoville 1991), in order to obtain L_{FIR} as an estimate of L_{bol} . From our high angular resolution millimeter data we can derive a central molecular gas mass of $m_{H_2}=7.5\times 10^9 M_\odot$. From Fig.7 in Young & Scoville (1991) we get a $L_{bol}=6.3\times 10^{10} L_\odot$, and dust temperature in the range of 40 to 60 K. *Secondly*, this can be compared to an estimate of L_{bol} via the well-known FIR-radio relation (Wunderlich & Klein 1988). This method is in good agreement with the result using the IRAS fluxes as shown by Wunderlich & Klein (1988) and summarized in Schinnerer et al. (1997). For I Zw 1 we can then use the 5 GHz radio flux to calculate L_{bol} . In a comparison to NGC 1068, Eckart et al. (1994) have provided evidence that most of the total 5 GHz radio flux can be attributed to the central starburst. By assuming:

$$L_{bol}[L_\odot] = 1.34 \times 10^{-7} \times (1.13 \times 10^{17} \times D[Mpc]^2 \times S_{5GHz}[mJy])^{0.791} \quad (4)$$

where S_{5GHz} is the flux density at 5GHz leading to a $L_{bol}=4.6\times 10^{10} L_\odot$ (Schinnerer et al. 1997). The two methods show a good agreement.

L_{Lyc} and L_K were estimated via

$$L_{Lyc}[L_\odot] = 3.57 \times 10^{19} \times F_{Br\gamma}[ergs^{-1}cm^{-2}] \times D[Mpc]^2 \quad (5)$$

and

$$L_K[L_\odot] = 1.14 \times 10^4 \times D[Mpc]^2 \times S_K[mJy] \quad (6)$$

$F_{Br\gamma}$ is the Br γ -line flux and S_K is the K band flux density (Genzel et al. 1995). These quantities have to be extinction corrected. The supernova rate ν_{SN} is calculated as

$$\nu_{SN}[yr^{-1}] = 3.1 \times 10^{-6} \times S_{5GHz}[mJy] \times D[Mpc]^2 \quad (7)$$

(Condon 1992). The adopted values for L_{Lyc} and L_K are discussed in the following section 5.2. All the luminosities as well as the resulting diagnostic ratios are listed in Table 4.

5.2. Properties of the Nuclear Starburst

If all the stellar K-band light were due to a very old stellar population the corresponding mass (derived as demonstrated in e.g. Thronson & Greenhouse 1988) - reddened or dereddened - would exceed the overall dynamical mass determined in section 3.3 by 1 to 2 orders of magnitude. Combined with the other evidence provided in the present paper and in Eckart et al. (1994) we conclude that a starburst (or at least enhanced star formation activity) takes place in the central region of I Zw 1 and therefore contributes a major fraction of the stellar near-infrared emission.

We assumed two cases for the model starburst: (a) the QSO nucleus is exclusively powered by a strong starburst and (b) only a fraction of the nuclear luminosity is due to a starburst which is located in the circumnuclear CO ring.

If the QSO nucleus is powered by a strong starburst alone, the entire K band and Lyman continuum luminosity is due to that starburst. As shown in section 4.2.1 there is little or no extinction in the direction of the nucleus for the Lyman continuum, so the same should be true for the K-band flux. In this scenario, no model reproduced the observed diagnostic emission ratios at any metallicity. In all of them fitting both the Lyman continuum and K-band luminosity results in bolometric luminosities two or three orders of magnitude larger than what is measured. Thus we rule out this possibility for the origin of the nuclear luminosity in I Zw 1.

If we assume, however, that only 20% of the K band flux is of stellar origin as it is suggested by the NIR spectrum (see section 4.2.2), these stars are located within the central 2" and are probably associated with the circumnuclear ring we found in the ^{12}CO line emission. For this stellar component we adopt an extinction of $A_V \approx 10^m$ as derived by Eckart et al. (1994) and discussed in section 4.2.2. Since the fraction of the Lyman continuum luminosity which is due to a starburst is not known, we tried to find the fraction of the Lyman continuum luminosity that would give a reasonable fit for the diagnostic ratios and would still agree with the observations of the Br γ flux.

This fit was obtained by maximizing a probability function proportional to $\exp(-\chi^2)$, here χ^2 is the sum of the 3 individual χ^2 -values calculated from the predicted and measured diagnostic ratios and their errors. L_K , L_{bol} , and ν_{SN} were kept fixed and L_{Lyc} was varied. The best fit is obtained if $\sim 0.5\%$ of the observed Lyman continuum luminosity and therefore also about $\sim 0.5\%$ of the Br γ line flux, used to derive the Lyman continuum luminosity, is due to the starburst. This fraction of the Lyman continuum luminosity is highly extinguished with respect to the rest of the emission (see section 4.2.1). The best fit to the data is a decaying starburst with a decay-time of 5×10^6 yrs. The model burst started about 4.5×10^7 yrs ago with a Salpeter IMF, and an upper mass cut-off of $\geq 90 M_\odot$. The present day stellar mass from this starburst is about $1.9 \times 10^{10} M_\odot$.

6. COMPARISON WITH STARBURST RINGS IN NEARBY GALAXIES

Starburst rings are observed in a variety of galaxies (Buta & Combes 1996, Maoz et al. 1996). These rings are thought to be formed due to the gravitational interaction of the stars and the gas. They are detected in the mid-infrared continuum, near-infrared colors, molecular gas line emission as well as in H α line emission. The overall structure of these rings is not entirely smooth, so they could also be formed by two spiral arms tightly twisted around the nucleus.

To test if the properties of the starburst ring in I Zw 1 are unique or more common we made a comparison (Table 5) to the starburst rings in the HII galaxy NGC 7552 (Schinnerer et al. 1997) and the Seyfert 1 NGC 7469 (Genzel et al. 1995), since these two rings were studied over the same wavelength range, and using the same starburst model. I Zw 1 is six times further away than NGC 7552, and three times more distant than NGC 7469. In the following comparison we refer to the data given in Table 5.

In NGC 7552 Schinnerer et al. (1997) were able to study the properties of the starburst ring in detail, since it is located at a distance of only 20 Mpc. The size of the ring is about 0.8 kpc, comparable to the ring detected in I Zw 1. The starburst is not smoothly distributed over the ring, rather there are regions of enhanced and lower star formation. The $10\mu\text{m}$ dust emission is also not smoothly distributed along the ring, suggesting a variation in dust mass or temperature. The ages of the different regions, as derived in Schinnerer et al. (1997), differ by about a factor of two. These individual starburst regions in the ring are about 1.5×10^7 yrs old (with a decay time of 5 Myrs) and appear to have a high upper mass cut-off. The overall bolometric luminosities of the two starburst rings are similar. The difference in the Lyman continuum and K band luminosities can be explained by the different ages, since with a decay-time of 5 Myrs, the Lyman continuum decreases as more and more of the massive stars die. The K-band flux, then increases since more K and M supergiants/giants form. Therefore, the overall properties of the circumnuclear starburst in I Zw 1 are similar to the burst in NGC 7552, except that it may be 2 to 3 times older in I Zw 1.

NGC 7469 harbors a Seyfert 1 nucleus which is surrounded by two tightly wound starbursting spiral arms (Tacconi et al. 1997), previously thought to be a starburst ring. The properties of the starburst are similar to the burst in NGC 7552. Since the $\text{Br}\gamma$ emission in NGC 7469 is knotty the starburst probably varies in age or strength between the different star formation sites. The "ring" is a bit larger than in NGC 7552, and is the size of that in I ZW 1. The bolometric luminosity in NGC 7469 is three times larger than that in NGC 7552. The two circumnuclear starbursts in NGC 7469 and I Zw 1 are comparable in size and also show similar starburst properties. As in the case of NGC 7552, the differences in Lyman continuum versus K band luminosity can be explained with different ages of the two starbursts, and the correspondingly different evolutionary stages of the stellar populations.

Summarizing, we find that the properties of the starburst "rings" are similar in all three galaxies. The differences in the total bolometric luminosity might be linked to the internal structure of the rings, and therefore the fueling of the individual starburst regions within the ring. The starburst in the ring of I ZW 1 is about three times older than those in the nearby objects NGC 7469 and NGC 7552. From this comparison it would seem that the molecular ring we detected in the $^{12}\text{CO}(1-0)$ line emission is hosting a starburst quite similar to those found in other circumnuclear rings. This could indicate that a fraction of the high luminosity observed for QSOs and Seyfert's is due to a circumnuclear starburst in the centers of their host galaxies, and that the AGNs are not alone responsible for the overall energy output in the optical/infrared. The contribution of the star formation activity to the bolometric luminosity can range from only about 10 % as in the case of I Zw 1 to about 50 % as observed for NGC 7469 (Genzel et al. 1995).

7. STAR FORMATION ACTIVITY IN THE I ZW 1 HOST GALAXY

In order to investigate the star formation activity in the spiral arms of the I Zw 1 host galaxy we use the population synthesis model as described in section 5.1, and compare the optical-infrared broad band spectra of the northwestern spiral arm in the I Zw 1 host galaxy and the western companion, to those of spiral galaxies, ellipticals and the disk and nucleus of NGC 7469 (Fig.9). From both the model calculations, and the bluer optical-infrared spectral energy distribution we find indications for enhanced star formation on the arm. This result is in agreement with the finding of Hutchings & Crampton (1990). From the optical colors and the absence of a definite Mg IIb band feature in the I Zw 1 disk these authors inferred that the host galaxy generally has an early type stellar population. For the companion we find V-K colors which are within their errors similar to those of ellipticals or spirals. We find that both the nucleus and the disk of I Zw 1 show properties of high redshift QSOs and their host galaxies. The indication of enhanced starburst activity from our population synthesis and the presence of significant amounts of molecular gas in the investigated area on the northwestern spiral arm 12 kpc off the nucleus suggests that star formation and not scattered light from the QSO nucleus is responsible for the blue disk colors.

7.1. Population synthesis

Although the observations of the I Zw 1 galaxy disk are of moderate S/N, it is possible to derive useful values for luminosities and the diagnostic ratios needed for the population synthesis model calculations. To get a consistent estimate of the luminosities we calculated all of them in 5" diameter circular apertures centered 9" W and 5" N of the nucleus right on the northwestern arm. We did not correct for reddening, since the average extinction in galaxy disks is often found to be low ($A_V \approx 1$; Frogel et al. 1978).

To estimate the supernova rate ν_{SN} we compared the 1.4 GHz flux of 6.22 ± 0.35 mJy measured by Barvainis & Antonucci (1989) in a 9" beam to the flux of 7.30 ± 0.45 mJy in the NRAO VLA Sky survey (NVSS) at 1.4 GHz (Condon et al. 1996) with a beam size of 45". We assume that the 1.1mJy difference in the two flux measurements is an upper limit for the emission from the disk with roughly the same size as the NVSS beam. To get the flux at 5 GHz we use a spectral index $\alpha = -0.88$ as derived by Barvainis & Antonucci (1989) for I Zw 1, and obtain a flux density value of 0.38mJy in a 45" beam. Since the NVSS beam encompasses most of the I Zw 1 host galaxy this value would correspond to an overall supernova rate of 0.07 yr^{-1} which is a few times the estimated overall supernova rate in the Milky Way of $(0.025 \pm 0.006) \text{ yr}^{-1}$ (Tammann, Löffler, Schröder 1994). The flux density value of 0.38mJy in a 45" beam corresponds to 5×10^{-6} Jy in a 5" beam at 5 GHz. This flux can be compared to the estimate of 0.5 mJy noise in a 45" beam at 1.4 GHz just off the disk (2' separation from the nucleus) in the NVSS map. This value results in 2×10^{-6} Jy in a 5" beam at 5 GHz. Using 5×10^{-6} Jy in a 5" beam as an upper limit, we obtain a supernova rate ν_{SN} of 0.001 yr^{-1} .

We derived the Lyman continuum luminosity by the $H\beta$ flux of approximately $10^{-15}\text{erg s}^{-1}\text{ cm}^{-2}$ over a $\sim 3'' \times 8''$ slit aperture in the off-nuclear spectrum by Hutchings & Crampton (1990), and a ratio of 36:1 for $H\beta:\text{Br}\gamma$. The resulting $\text{Br}\gamma$ line flux is $\sim 2.3 \times 10^{-17}\text{erg s}^{-1}\text{ cm}^{-2}$ in a $5''$ aperture. This is clearly below our upper limit of $3.3 \times 10^{-15}\text{erg s}^{-1}\text{ cm}^{-2}$ (3σ) derived from our spectroscopic imaging data. The derived value leads to $L_{\text{Lyc}} = 4.9 \times 10^7 L_{\odot}$.

From the IRAC2 K band image we obtain an average value for the flux density of $1.2 \times 10^{-4}\text{Jy}$ in a $5''$ diameter aperture. This translates into a K band magnitude of 16.8^{mag} , and gives a K band luminosity of $L_K = 8.1 \times 10^7 L_{\odot}$.

To get an estimate of the bolometric luminosity we used the CO-IR relation as described in section 5.1. From our $5''$ channel maps with a spectral resolution of 10 km/s we get an $I_{\text{CO}} = 3.35\text{ K km/s}$ with $\Delta v \sim 40\text{ km/s}$ and $S \sim 20\text{ mJy}$. Correcting for the beam filling factor assuming a $15''$ diameter disk, this converts into a molecular H_2 mass of about $3.1 \times 10^8 M_{\odot}$, and leads to $L_{\text{bol}} = 5.0 \times 10^9 L_{\odot}$ (assuming a dust temperature in the range of 30 to 40 K).

Assuming solar metallicity we can now use these values and their diagnostic ratios to determine the properties of a single underlying starburst (see Fig.8 in Genzel et al. 1995, or Fig.10 in Schinnerer et al. 1997). The diagnostic ratios calculated from the above values indicate a young decaying starburst with an age of $\sim 1.3 \times 10^7\text{ yrs}$ and a moderate upper mass cut-off of $m_u \sim 15 M_{\odot}$. The ratios are also in agreement with an old ($\sim 10^{10}\text{ yrs}$), constant starburst and an upper mass cut-off of 20 to $30 M_{\odot}$. In any case our estimates of the diagnostic ratios indicate active star formation in the northwestern arm of the I Zw 1 host galaxy disk.

7.2. Broad band spectra

From our IRAC2 H and K (Fig.7) band images as well as the V and I band HST images (see Fig.2 (Plate 1)) we obtained flux densities (and the corresponding magnitudes) in $5''$ circular apertures centered on the northwestern arm ($9''$ W and $5''$ N), on the western companion, and on the nucleus of I Zw 1 itself. We compared these data to the mean spectra of spiral galaxies, ellipticals, and the disk and nucleus of NGC 7469 (Fig.9).

The spiral galaxy data for representative RC3 types 0 to 2 (S0 - Sab) and 6 to 8 (Scd - Sdm) were taken from de Jong (1996). We took the data on ellipticals from Goudfrooij et al. (1994) for the B, V, and I band and from Silva & Elston (1994) for the J, H, and K band. The galaxies NGC 3377, NGC 3379, and NGC 5813 are listed by both groups. For these three objects the H band magnitudes were derived using the mean NIR colors of the other ellipticals in the same sample. In Fig.9 we display the combined data. The data on the disk of NGC 7469 are taken from Kotilainen and Ward (1994) measured in a circular annulus of $6''$ to $12''$ diameter centered on the nucleus. For the nucleus the data are from Kotilainen, Ward, Williger (1993) for V and I band, and Kotilainen et al. (1992) for H and K band measured in a $3''$ circular aperture centered on the nucleus.

In addition we checked the relative calibration of the V and I band data on I Zw 1 using the visible (380–600 nm) and red (660–965 nm) spectra of the nucleus published by Hutchings

& Crampton (1990) and Osterbrock, Shaw & Veilleux (1990). Hutchings & Crampton (1990) also provide an absolute calibration of their optical spectrum and give a calibrated R band map. These spectra are almost continuous in wavelength range and allow us to estimate the spectral shape of the nucleus ranging from the V to I band. The data are consistent with the V and I band calibration provided by the HST, indicating that the I band flux density dip in the broad band spectrum of the nucleus of I Zw 1 is real. This dip spectrally separates the blue optical QSO nucleus from the red dusty circumnuclear environment in which the QSO nucleus is embedded.

Comparing the broad band spectra of spirals and ellipticals to those we obtained on the off-nuclear regions in I Zw 1, and the companion we find that in general, the optical colors of the spiral arm and the companion are bluer than what expected for normal (nearby) ellipticals and spiral galaxies. Their spectra have shapes quite comparable to those of spirals and ellipticals. The spectrum of the spiral arm (and within the errors also the spectrum of the companion) is as blue as or bluer than the spectrum of central 3" of the Seyfert I galaxy NGC 7469, where a substantial fraction of the light is originating in a circumnuclear starburst (Genzel et al. 1995).

An indication that host galaxies of QSOs at higher redshift may, in general, be bluer than what expected for normal (nearby) ellipticals and spiral galaxies is given by several authors. Hutchings and Neff (1997) find blue host colors for 2 out of 4 objects in the redshift range of $z=0.6$ to 3.0 . Rönback et al. (1996) find blue hosts in 16 out of 21 QSOs and quasars in the redshift range of $z=0.4$ to 0.8 . The blue disk colors we find for the I Zw 1 host demonstrates that not only the spectral line emission of the I Zw 1 QSO nucleus shows properties of high-redshift QSOs (the blue shifted CIV line - Buson & Ulrich 1990 - and the blue shifted SiVI line - this paper in section 4.2.1), but also that the I Zw 1 host galaxy has structural and broad band spectral properties similar to those of high redshift QSO host galaxies.

The bluer colors may indicate enhanced star formation, and are consistent with the interpretation of Hutchings & Crampton (1990) that the disk generally shows an early type population. This conclusion is also consistent with the result of our starburst analysis in the previous section. The star formation activity, as well as the presence of molecular material within the disk (section 3.1) and on the arm, indicates that at least in this region – 12 kpc off the nucleus – it is most likely star formation that is responsible for the blue disk colors. An alternative explanation for the blue disk colors might be a contribution of scattered light from the nucleus as in the case of 3C 234 (Tran, Cohen and Goodrich 1995) or Cygnus A (Ogle et al. 1997). How large such a contribution might be has to be investigated by high angular resolution spectro-polarimetry of the I Zw 1 host galaxy.

8. SUMMARY AND CONCLUSIONS

Our study of the host galaxy of I Zw 1 covers the wavelength range from the radio to the optical. We have mapped the distribution of molecular gas in the QSO host in its

$^{12}\text{CO}(1-0)$ line emission. The total molecular gas mass is of the order of $9 \times 10^9 M_{\odot}$ with more than 2/3 of it located within the central $3.3''$. This amounts to about 20% of the dynamical mass in the center. Modeling the disk dynamics suggests an inclination of $38^{\circ} \pm 5^{\circ}$. The mass balance for the nucleus results in a $\frac{N_{\text{H}_2}}{I_{\text{CO}}}$ -conversion factor in general agreement with $2 \times 10^{20} \text{ cm}^{-2} \text{ K}^{-1} \text{ km}^{-1} \text{ s}$ found for molecular gas in our Galaxy and many nearby external galaxies.

We have detected the spiral arms of the host in molecular line emission, and find a circumnuclear ring with a diameter of 1.8 kpc ($1.5''$). NIR spectroscopy of the central $3''$ has revealed the presence of a prominent stellar component in this region. Combined with available radio data we conclude that a young, massive, and decaying starburst is associated with this circumnuclear ring. The properties of this starburst ring are similar to the ones observed in other sources with nuclear activity. These similarities indicate that these rings may be a common phenomenon and contribute a significant fraction to the central luminosity.

Our H and K band images as well as V and I band HST images, together with data taken from the literature, show that the star formation in the *disk* of I Zw 1 is enhanced as well. A comparison with broad band spectra of spiral galaxies, ellipticals and the nucleus and disk in NGC 7469 clearly suggests that the north western arm in the I Zw 1 host galaxy is bluer than expected. The enhanced star formation in the host may indicate tidal interaction with a companion that shows an energy distribution similar to ellipticals. The companion's optical spectrum is also marginally bluer than expected. A similar behaviour is found for host galaxies of intermediate redshift QSOs and quasars.

In summary we find that both the nucleus and the disk of I Zw 1 show properties of higher redshift QSOs and their host galaxies. Further studies of I Zw 1 will therefore be useful to probe and understand properties of QSOs and their host galaxies at higher redshift.

We are grateful to the ESO/MPG 2.2m telescope staff and staff of IRAM, especially D. Downes, for their support and hospitality. We thank the staffs of the 3.5m telescope at Calar Alto and the WHT for their excellent support. We thank Th. Boller, R. Fosbury and N. Scoville for their comments and the helpful discussions as well as our referee P. Maloney for his comments and help to improve this manuscript. We are especially grateful to N. Thatte, L.E. Tacconi-Garman and the rest of the MPE 3D team for taking the H and K band NIR spectra. We also thank M. Löwe and A. Quirrenbach for taking the H and K band IRAC2 images at the ESO/MPG 2.2 telescope.

REFERENCES

- Ali, B., DePoy, D.L., Sellgren, K., Carr, J.S., Gatley, I., Merrill, K.M., 1995, Bull. American Astron. Soc., 187, #66.02
- Barvainis, R., 1990, Ap. J., 353, 419.
- Barvainis, R., Antonucci, R., 1989, Ap. J. Supp., 70, 257.
- Barvainis, R., Alloin, D., Antonucci, R., 1989, Ap. J. (Letters), 337, L69.
- Barvainis, R., Maloney, P., Antonucci, R., Alloin, D., 1997, Ap. J., 484, 695.
- Boller, T., Brandt, W.N., Fink, H., 1996, Astron. Astrophys., 305, 53.
- Bothun, G. D., Heckman, T. M., Schommer, R. A., Balick, B., 1984, A. J., 89, 1293.
- Buson, L.M., and Ulrich, M. H., 1990, Astron. Astrophys., 240, 247.
- Buta, R., Combes, F., 1996, Fund. Cosmic Physics, Vol.17 p.95
- Condon, J.J., Hutchings, J.B., Gower, A.C., 1985, A. J., 90, 1642.
- Condon, J.J., 1992, Ann.Rev.Astr.Ap., 30, 575.
- Condon, J.J., Cotton, W.D., Greisen, E.W., Yin, Q.F., Perley, R.A., Broderick, J.J. 1996, NCSA Astronomy Digital Image Library
- Dallier, R., Boisson, C., Joly, M., 1996, Astron. Astrophys. Suppl., 116, 239.
- de Jong, R.S., 1996, Astron. Astrophys., 313, 377.
- Dickel, J.R., 1976, in Methods of experimental Physics, Part 12c, ed. M. Marton, Academic Press, New York, San Francisco
- Doyon, R., Puxley, P.J., Wright, G.S., 1992, Ap. J., 397, 117.
- Doyon, R., Joseph, R.D., Wright, G.S., 1994, Ap. J., 421, 101.
- Eckart, A., 1996 in *Proc. of IAU Symposium 170, CO: Twenty-five Year of Millimeter-wave Spectroscopy*, Dordrecht:Reidel, p.257-264.
- Eckart, A., Cameron, M., Boller, Th., Krabbe, A., Blietz, M., Nakai, N., Wagner, S.J., Sternberg, A., 1996, Ap. J., 472, 588.
- Eckart, A., Cameron, M., Jackson, J.M., Genzel, R., Harris, A.I., Wild, W., Zinnecker, H., 1991, Ap. J., 372, 67.
- Eckart, A., Downes, D., Genzel, R., Harris, A.I., Jaffe, D.T. and Wild, W., 1990, Ap. J., 348, 434.
- Eckart, A., van der Werf, P.P., Hofmann, R., Harris, A.I., 1994, Ap. J., 424, 627.
- Edelson, R.A., Malkan, M.A., 1986, Ap. J., 308, 59.
- Frogel, J.A., Persson, S.E., Aaronson, M., Matthews, K., 1978, Ap. J., 220, 75.
- Gehrz, R.D., Sramek, R.A., and Weedman, D.W., 1983, Ap. J., 267, 551.
- Genzel, R., et al., 1997, submitted

- Genzel, R., Weitzel, L., Tacconi-Garman, L.E., Blietz, M., Krabbe, A., Lutz, D., Sternberg, A., 1995, *Ap. J.*, 444, 129.
- Goudfrooij, P., Hansen, L., Jørgensen, H.E., Nørgaard-Nielsen, H.U., de Jong, T., van den Hoek, L.B., 1994, *Astron. Astrophys.*, 104, 179.
- Guilloteau, S., et al. 1992, *Astron. Astrophys.*, 262, 624.
- Halpern, J.P., and Oke, J.B., 1987, *Ap. J.*, 312, 91.
- Heeschen, D.S., 1961, *Ap. J.*, 133, 322.
- Hunt, L.K., Malkan, M.A., Salvati, M., Mandolesi, N., Palazzi, E., Wade, R., 1997, *Ap. J. Supp.*, 108, 229.
- Hutchings, J.B., Crampton, D., 1990, *A. J.*, 99, 37.
- Hutchings, J.B., Neff, S.G., 1997, *Ap. J.*, 113, 550.
- Kawara, K., Nishida, M., Gregory, B., 1990, *Ap. J.*, 352, 433.
- Kleinmann, S.G., Hall, D.N.B., 1986, *Ap. J. Supp.*, 62, 501.
- Kotilainen, J.K., Ward, M.J., 1994, *M.N.R.A.S.*, 266, 953.
- Kotilainen, J.K., Ward, M.J., Williger, G.M., 1993, *M.N.R.A.S.*, 263, 655.
- Kotilainen, J.K., Ward, M.J., Boisson, C., De Poy, D.L., Bryant, L.R., Smith, M.G., 1992, *M.N.R.A.S.*, 256, 125.
- Kovo & Sternberg 1997, in preparation.
- Krabbe, A., Sternberg, A., and Genzel, R., 1994, *Ap. J.*, 425, 72.
- Kruper, J.S., Urry, C.M., and Canizares, C.R., 1990, *Ap. J. Supp.*, 74, 347.
- Lançon, A., Rocca-Volmerange, B., 1996, *New Astronomy*, 1, 215
- Laor, A., Buell, T.J., Green, R.F., Boroson, T.A., 1997, *Ap. J.*, 489, ., in press
- Larson, R. B., Tinsley, B. M., 1978, *Ap. J.*, 219, 46.
- Leighly, K.M., Mushotzky, R.F., Nandra, K., Forster, K., 1997, *Ap. J. L.*, accepted
- Leitherer, C., 1996, in *ASP.conf. series Vol.98*, p. 373.
- Lord, S., 1992, *NASA Technical Memorandum 103957*, Ames Research Center, Moffett Field, CA
- Maloney, P., Black, J.H., 1988, *Ap. J.*, 325, 389.
- Maoz, D., Barth, A.J., Sternberg, A., Filippenko, A.V., Ho, L.C., Macchetto, F.D., Rix, H.-W., Schneider, D.P., 1996, *A. J.*, 111, 2248.
- Mas Hesse, J.M., and Kunth, D., 1991, *Astr.Ap.Suppl* 88, 399
- McGaugh, S.S., de Blok, W.J.G., 1997, *Ap. J.*, 481, 689.
- McLeod, K.K., Rieke, G.H., 1995, *Ap. J.*, 441, 69.

- Meynet, G., Maeder, A., Schaller, G., Schaerer, D., Charbonnel, C., 1994, *Astron. Astrophys. Suppl.*, 103, 97.
- Nicholson, R.A., Bland-Hawthorn, J., Taylor, K., 1992, *Ap. J.*, 387, 503.
- Norman, C., Scoville, N., 1988, *Ap. J.*, 332, 124.
- Ogle, P.M., Cohen, M.H., Miller, J.S., Tran, H.D., Fosbury, R.A.E., Goodrich, R.W., 1997, *Ap. J. (Letters)*, 482, L37.
- Osterbrock, D.E., Shaw, R.A., and Veilleux, S., 1990, *A. J.*, 352, 561.
- Osterbrock, D.E., 1989, *Astrophysics of Gaseous Nebulae and Galactic Nuclei*,
- Osterbrock, D.E., 1993, *Ap. J.*, 404, 551.
- Quillen, A.C., de Zeeuw, P.T., Phinney, E.S., Phillips, T.G., 1992, *Ap. J.*, 391, 121.
- Quillen, A.C., Graham, J.R., Frogel, J.A., 1993, *Ap. J.*, 412, 550.
- Rieke, G. H., Lebofsky, M. J., Thompson, R. I., Low, F. J., Tokunaga, A. T., 1980, *Ap. J.*, 238, 24.
- Rieke, G. H., Loken, K., Rieke, M. J., Tamblyn, P., 1993, *Ap. J.*, 412, 99.
- Rieke, G.H., Lebofsky, M.J., and Walker, C.E., 1988, *Ap. J.*, 325, 679.
- Rönback, J., van Groningen, E., Wanders, I., Örndahl, E., 1996, *M.N.R.A.S.*, 283, 282.
- Rubin, V.C., Burstein, D., Ford, W.K., Thonnard, N., 1985, *Ap. J.*, 289, 81.
- Rubio, M., Lequeux, J., Boulanger, F., 1993, *Astron. Astrophys.*, 271, 9.
- Salpeter, E. E., 1955, *Ap. J.*, 121, 161.
- Sanders, D.B., Tubbs, A.D., 1980, *Ap. J.*, 235, 803.
- Sanders, D.B., Soifer, B.T., Elias, J.H., Madore, B.F., Matthews, K., Neugebauer, G., and Scoville, N., 1988, *Ap. J.*, 325, 74.
- Schaerer, D., Maynet, G., Maeder, A., Schaller, G., 1993, *Astron. Astrophys.*, 274, 1012.
- Schinnerer, E., Eckart, A., Quirrenbach, A., Böker, T., Tacconi-Garman, L.E., Krabbe, A., Sternberg, A., 1997, *Ap. J.*, 488, 174.
- Shields, J., 1993, *A. J.*, 419, 181.
- Silva, D.R., Elston, R., 1994, *Ap. J.*, 428, 511.
- Smith, E.P., Heckman, T.M., Bothun, G.D., Romanishin, W., Balick, B., 1986, *Ap. J.*, 306, 64.
- Solomon, P.M., Downes, D., Redford, S.J.E., Barrett, J.W., 1997, *Ap. J.*, 478, 144.
- Sparke, L.S., 1996 *Ap. J.*, 473, 810.
- Strong, A. W., et al. 1987, *Proc. 20th Intern. Cosmic Ray Conf.*, I, 125
- Tacconi et al. 1997, in preparation

- Tacconi, L.J., Genzel, R., Blietz, M., Cameron, M., Harris, A.I., Madden, S., 1994, *Ap. J. (Letters)*, 426, L77.
- Tacconi-Garman, L.E., Sternberg, A., Eckart, A., 1996, *A. J.*, 112, 918.
- Tammann, G.A., Löffler, W., Schröder, A., 1994, *Ap. J. Supp.*, 92, [487
- Thatte, N.A., Kroker, H., Weitzel, L., Tacconi-Garman, L.E., Tecza, M., Krabbe, A., Genzel, R., 1995, *Proc. SPIE Vol. 2475*, 228
- Thronson, H.A. Jr., Greenhouse, M.A., 1988, *ApJ327671*
- Tran, H.D., Cohen, M.H., Goodrich, R.W., 1995, *AJ1102597*
- Weitzel, L., Krabbe, A., Kroker, H., Thatte, N., Tacconi-Garman, L. E., Cameron, M., Genzel, R., 1996, *Astron. Astrophys. Suppl.*, 119, 531.
- van Dishoeck, E.F., Black, J.H., 1987, *NATO ASI series*, vol. 210, 241on *Physical*
- Véron-Cetty, M.P., Véron, P., 1991, *A Catalogue of Quasar and Active Nuclei (5th Edition)*, Munich: European Southern Observatory
- Wilson, C.D., and Reid, I.N., 1991, *Ap. J. (Letters)*, 366, L11-L14.
- Wunderlich, E., Klein, U., 1988, *Astron. Astrophys.*, 206, 47.
- Xie, S., Young, J., Schloerb, F.P., 1994, *Ap. J.*, 421, 434.
- Young, J.S. and Scoville, N.Z., 1991, *Ann.Rev.Astron.Astrophys.*, 29, 581.

Table 1: $^{12}\text{CO}(1-0)$ flux distribution in I Zw 1

	FWHM	S_{obs}	T_{obs}	T_{real}	Distribution
nucleus	3.3''	0.056 Jy	0.0117 K	0.551 K	Gaussian
disk	9.0''	0.022 Jy	0.0046 K	0.033 K	Gaussian
disk	12.0''	0.022 Jy	0.0046 K	0.005 K	flat

Observed flux density and main beam brightness temperature of the 30m flux measurements as well as the source size corrected temperatures assuming sizes for the disk and nucleus as given.

Table 2: Molecular mass distribution in I Zw 1

	Δv [km s $^{-1}$]	I_{CO} [K km s $^{-1}$]	$N(\text{H}_2)$ [10^{21}cm^{-2}]	A [kpc 2]	M_{H_2} [$10^9 M_{\odot}$]
nucleus (3.3'')	380	209.4	42	11.8	7.5
disk (9.0'')	310	10.2	2.0	88.6	2.7
disk (12.0'')	310	1.6	0.3	157.5	0.7

Derived mass of molecular hydrogen for the nuclear and disk. The velocity widths are measured peak-to-peak for the disk component and FZW for the nucleus.

Table 3: Integrated NIR line fluxes of I Zw 1

	wavelength [μm]	peak intensity [$10^{-15} \text{ W m}^{-2} \mu\text{m}^{-1}$]	flux [$10^{-18} \text{ W m}^{-2}$]	
		3D	3D	FAST
Pa α	1.8751	26.9 \pm 0.7	284 \pm 12	
Br γ	2.1665	2.4 \pm 0.7	26 \pm 8	
Br δ	1.9445	1.5 \pm 0.7	3.7 \pm 1.8	
H ₂ S(1)	2.1218	<0.15	<2.4	0.68 \pm 0.20
SiVI	1.9615	1.4 \pm 0.7	3.5 \pm 1.8	< 3.0
AlIX	2.040	0.7 \pm 0.7	3.2 \pm 3.2	
CO 6-3	1.6185	2.1 \pm 0.7	-4.6 \pm 1.5	

The peak line intensities taken from the spectrum in Fig.8 and integrated line fluxes in a 3'' aperture. The 3σ errors for both the peak and the integral values are given. For comparison the line fluxes measured with FAST (Eckart et al. 1994) are listed in the 4th column as well. Within the uncertainties they are in agreement with the new data presented here.

Table 4: Luminosities and diagnostic ratios for nuclear starburst models

	model (a)	model (b)	fit
S_K [mJy]	69.2	13.84	
$F_{Br\gamma}$ [10^{-18} Wm^{-2}]	26	~ 0.04	
S_{5GHz} [mJy]	2.2	2.2	
L_{Bol} [$10^{10} L_{\odot}$]	6.3	6.3	100
L_K [$10^{10} L_{\odot}$]	4.70	1.61	1.61
L_{LYC} [$10^9 L_{\odot}$]	54.3	0.23	1.19
ν_{SN} [yr^{-1}]	0.41	0.41	2.66
$\frac{L_{bol}}{L_{Lyc}}$	1.2	273.9	840.4
$\log(\frac{L_K}{L_{Lyc}})$	-0.06	1.84	1.13
$\frac{10^9 \nu_{SN}}{L_{Lyc}}$	0.008	1.735	2.236
t [10^7 yr]		3.0 - 6.0	4.4
m_u [M_{\odot}]		≥ 90	120

Flux densities and line fluxes used to derive the luminosities and supernova rate of the circumnuclear starburst in I Zw 1. The calculated diagnostic ratios and the ratios of a good fit for model (b) are also given. We assumed a distance of 244 Mpc and an $A_V=10^{mag}$ for model (b) and no extinction for model (a). The models as well as the predicted values are described in the text.

Table 5: Comparison to other starburst rings

	NGC 7552	NGC 7469	I Zw 1
Type	LINER/H II	Seyfert 1	QSO/Sey 1
Distance	20 Mpc	66 Mpc	244 Mpc
Size	17 kpc	20 kpc	~ 30 kpc
Ring Diameter	1 kpc	1 kpc	1.8 kpc
L_{bol} [$10^{10}L_{\odot}$]	3	10	6.3
L_K [10^9L_{\odot}]	0.7	3	16
L_{Lyc} [10^9L_{\odot}]	2.8	9.5	0.3
ν_{SN} [yr^{-1}]	0.1	0.4	0.4
$\frac{L_{bol}}{L_{Lyc}}$	10	28 - 38	210
$\frac{L_K}{L_{Lyc}}$	0.24	~0.3	53
$\frac{10^9\nu_{SN}}{L_{Lyc}}$	0.034	0.049	1.33
m_u [M_{\odot}]	≈ 100	≤ 100	≥ 90
t_{burst} [Myr]	~ 15	~ 15	~ 45
type	dec.	dec. (?)	dec.

Properties of the starburst rings in NGC 7552 taken from Schinnerer et al. (1997) and in NGC 7469 from Genzel et al. (1995). The data for I Zw 1 are presented in this paper.

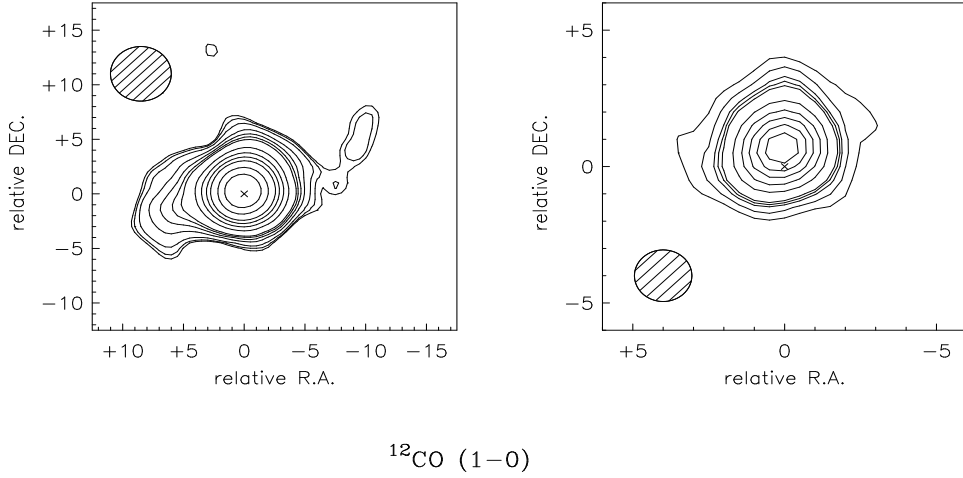


Fig. 1.— Integrated maps of the $^{12}\text{CO}(1-0)$ line with an angular resolution of $5''$ corresponding to 5.9 kpc (left, Fig.1a) and $1.9''$ corresponding to 2.2 kpc (right, Fig.1b). The contour levels are 0.077, 0.078, 0.080, 0.085, 0.090, 0.095, 0.10, 0.125, 0.15, 0.175, 0.20, 0.25, 0.30, 0.35 Jy/beam for the left map and 0.04, 0.06, 0.08, 0.09, 0.10, 0.15, 0.20, 0.25, 0.30, 0.35 Jy/beam for the right map.

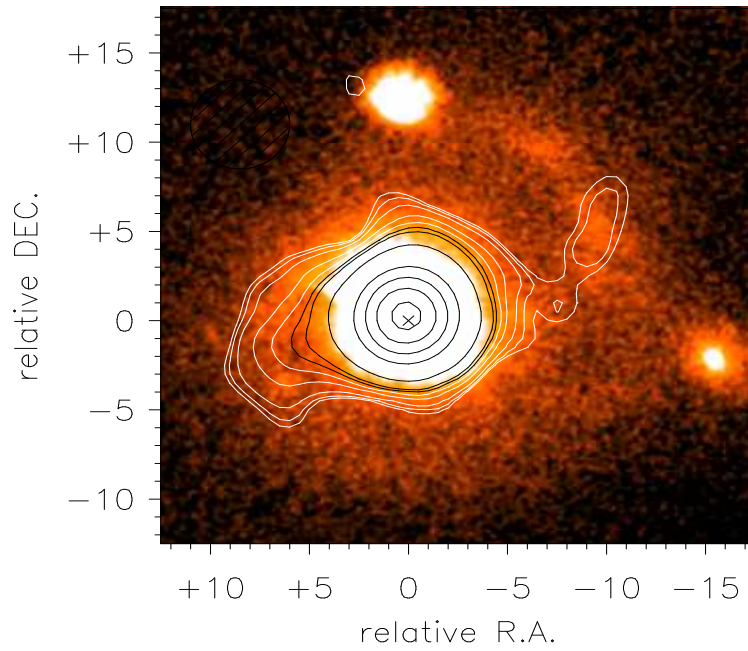


Fig. 2.— Integrated maps of the $^{12}\text{CO}(1-0)$ line with an angular resolution of $5''$ corresponding to 5.9 kpc. The contour levels are 0.077, 0.078, 0.080, 0.085, 0.090, 0.095, 0.100, 0.125, 0.150, 0.175, 0.200, 0.250, 0.300, 0.350, 0.400 Jy/beam. Underlying the I band HST image of I Zw 1 convolved to a resolution of $2''$ for better comparison.

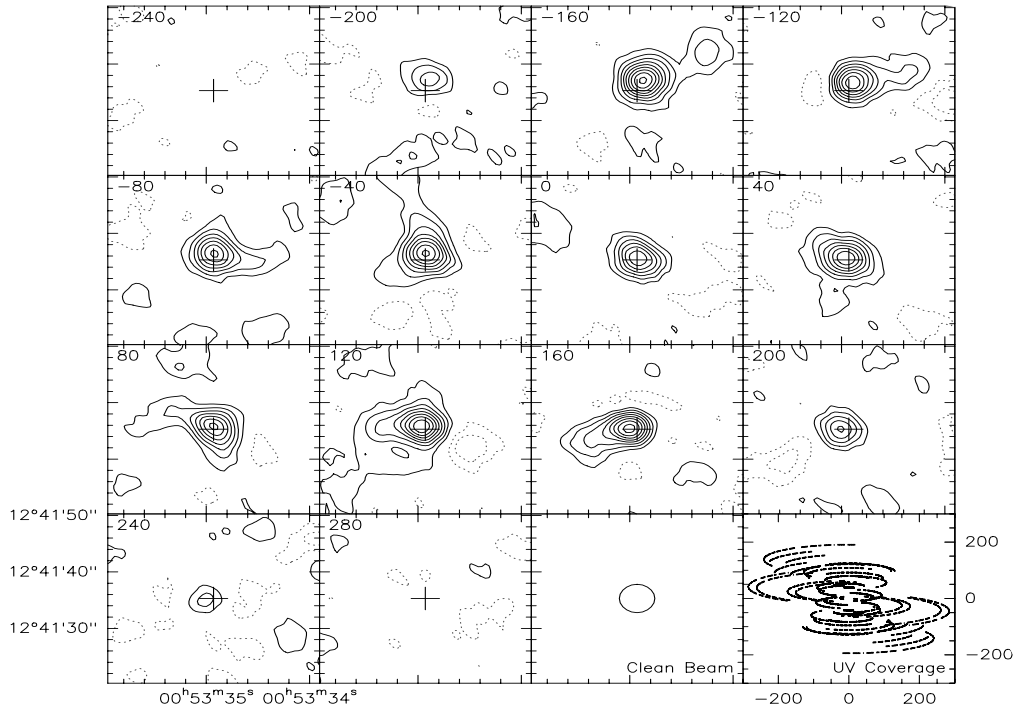


Fig. 3.— Channel maps of the ^{12}CO (1-0) line emission with a spectral resolution of 40 km/s and an angular resolution of $5''$. The contour levels are in steps of 5 mJy/beam. Clean beam and uv coverage are plotted as well. The central velocity of each channel with respect to the systemic velocity is indicated in each image. The extended emission of a rotating disk is clearly detected.

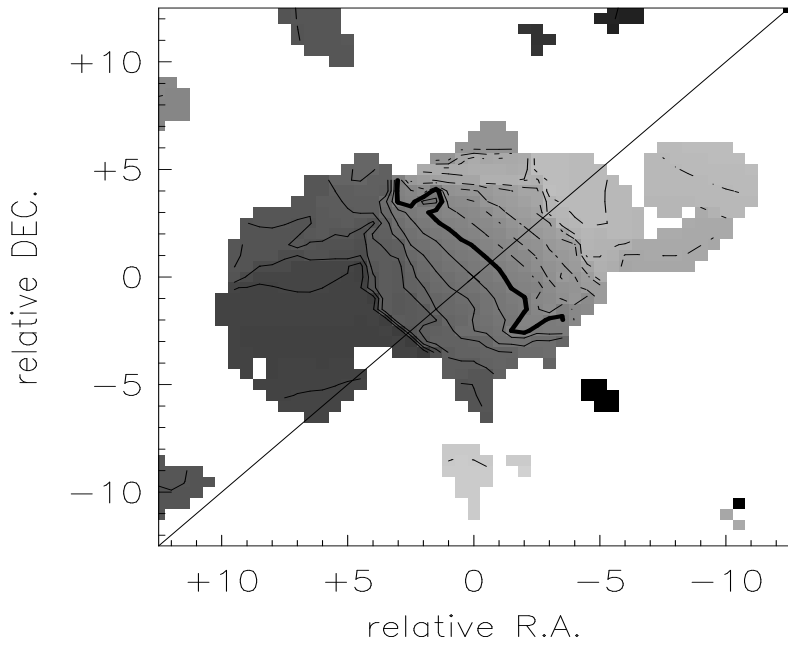


Fig. 4.— Velocity field of the ^{12}CO (1-0) line emission with an angular resolution of $5''$. The contours are -240 km/s, -220 km/s, -200 km/s, ... , 0 km/s, ... , 240 km/s. Light grey shading and dashed contour levels correspond to negative velocities. The thick dark line is the 0 km/s contour. For reference the kinematic major axis has been included as well.

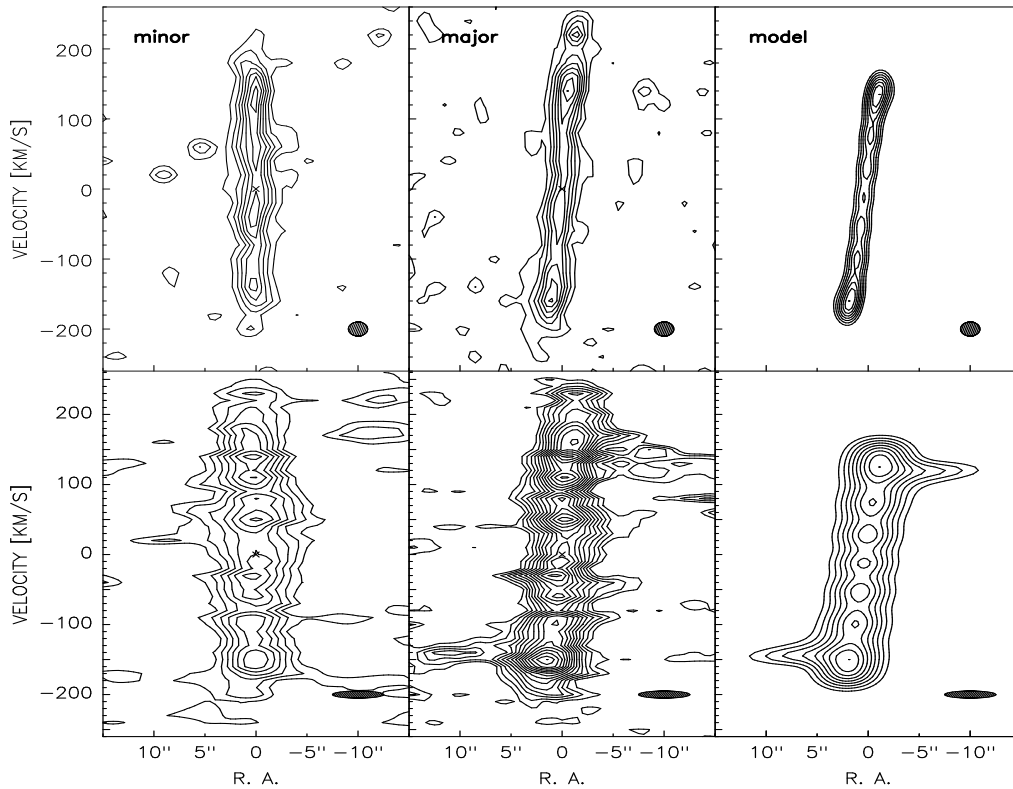


Fig. 5.— pv-diagrams of the $^{12}\text{CO}(1-0)$ line emission along the kinematic minor and major axis for the high angular resolution map (1.9'' FWHM; 20 km/s) (top) and low angular resolution map (5'' FWHM; 10 km/s) (bottom). In addition the modelled pv-diagrams for the major axis are plotted on the right. The contour levels are equally spaced with separations 10% starting at the 35% (top and bottom left), 10% starting at the 30% level (top middle and right), 5% starting at the 30% (bottom middle), and 10% starting at the 20% (bottom right) of the peak brightness.

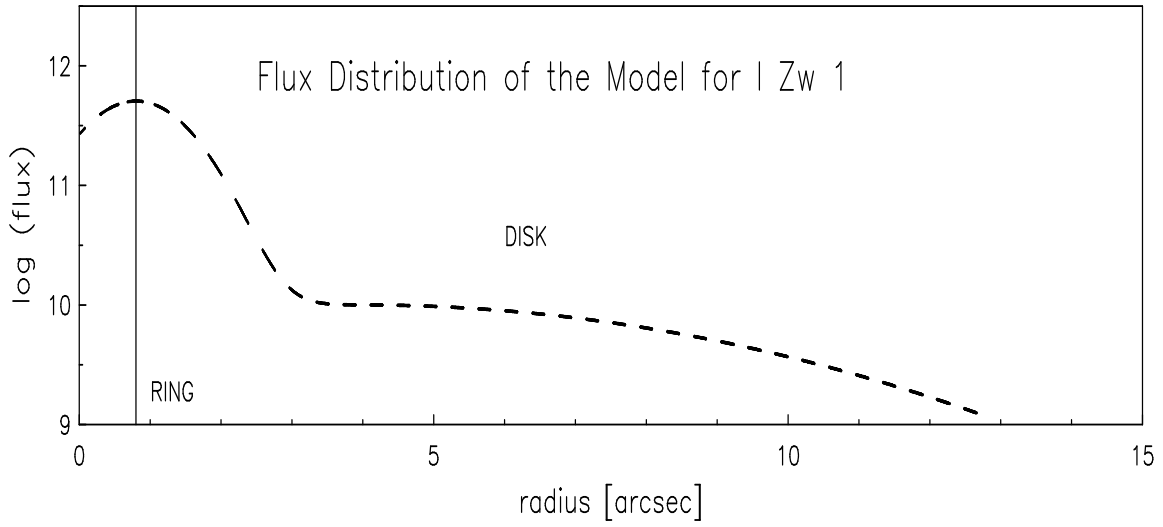


Fig. 6.— The $^{12}\text{CO}(1-0)$ line flux distribution as a function of radius for the derived model. A nuclear ring with a radius of $0.8''$ is superposed on an underlying and much less luminous disk.

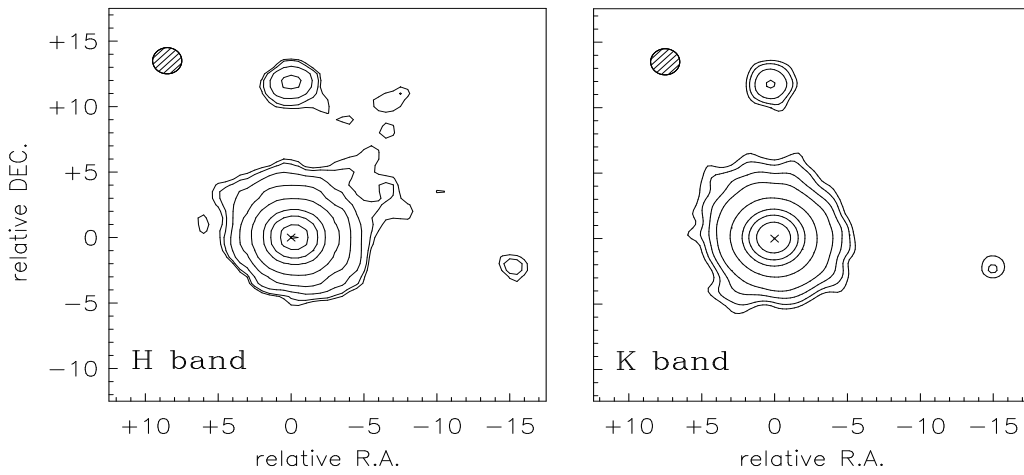


Fig. 7.— Maps of the H band (left) and K band (right) continuum emission. Contour levels are 1.2, 1.33, 1.7, 2.7, 5.3, 16.7, 33, 67, 93 % for the H band and 0.35, 0.47, 0.7, 1.1, 2.3, 3.5, 11.7, 23.5, 47, 95 % of the peak brightness for the K band map. As indicated by the beam in the upper left hand corner the angular resolution in both images is $2''$. In both images the star to the north, the companion galaxy to the west as well as the extended emission of the central disk are apparent.

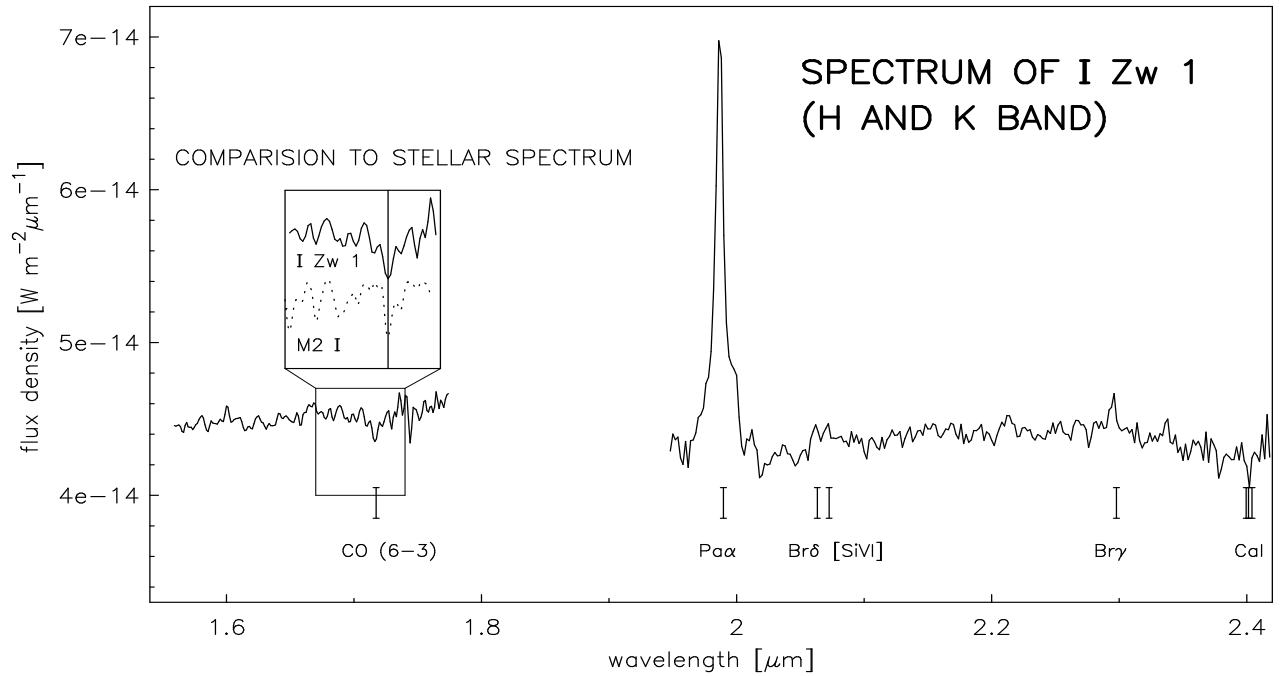


Fig. 8.— NIR-spectrum of I Zw 1 in the H and K band (1.58 - 1.78 μm and 1.95 - 2.40 μm). The spectrum includes light from the inner 3'' of the nucleus. For the CO(6-3) overtone a comparison to a stellar spectrum of an M2 I star convolved to the resolution of the measured I Zw 1 spectrum (Dallier et al. 1996) is shown. The positions of other prominent detected lines are indicated.

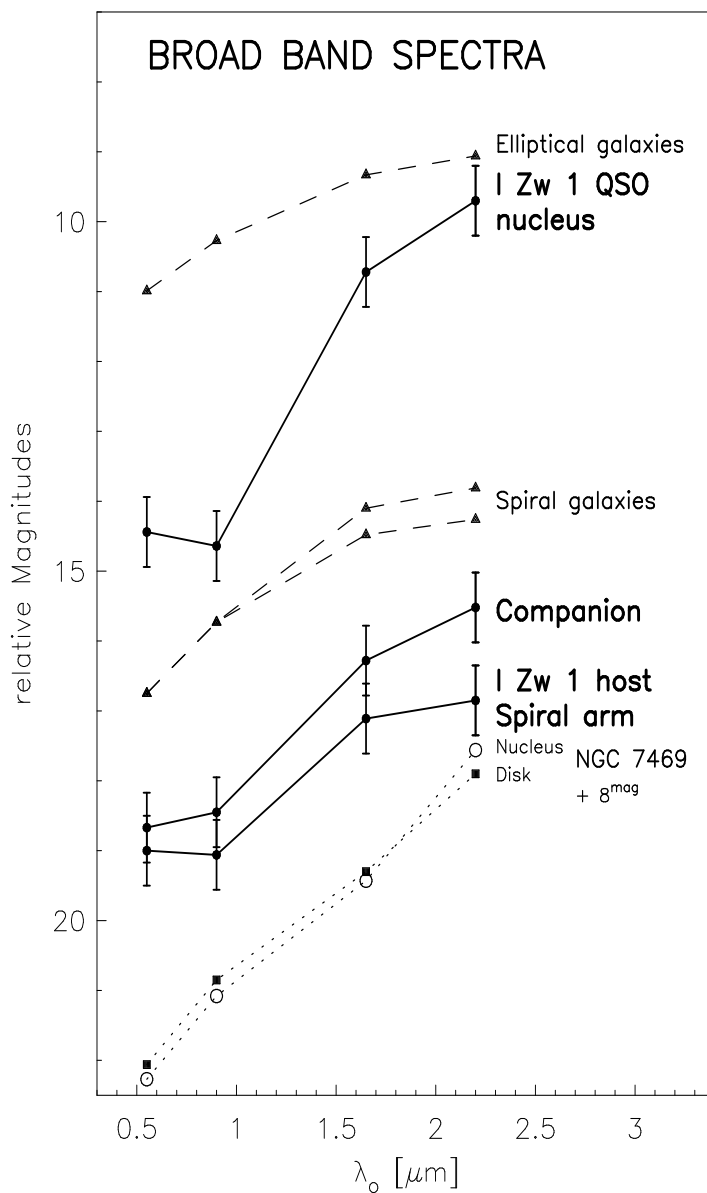


Fig. 9.— Broad band spectra of the northwestern arm ($9''$ W and $5''$ N), on the western companion, and on the nucleus of I Zw 1 itself. For comparison we show mean spectra of spiral galaxies (top curve: S0 - Sab; bottom curve: Scd - Sdm; de Jong 1996), ellipticals (Goudfrooij et al. 1994; Silva & Elston 1994), and the disk and nucleus of NGC 7469 (Kotilainen and Ward 1994 and references therein). The spectrum of NGC 7469 was shifted by $+8^{mag}$ for display purposes. The estimated errors on the I Zw 1 measurements (including positioning of aperture) are $\pm 0.5^{mag}$. See text for further information.